International Journal of Micro Air Vehicles

ORIGINAL RESEARCH ARTICLE

Open Access

https://doi.org/10.48130/mav-0026-0022

International Journal of Micro Air Vehicles **2026**, 18: e019

Composite angular rate constrained control for unmanned helicopter attitude systems with consideration of flapping dynamics via a fully actuated system approach

Zhenhua Kong[1], Peng Li[2], Fangzheng Li[1] and Zhenhua Zhao[1*]

[1] *College of Automation Engineering, Nanjing University of Aeronautics and Astronautics, Nanjing 211106, China*
[2] *National key laboratory on near-surface detection, Beijing 100072, China*
* Correspondence: zzh@nuaa.edu.cn (Zhao Z)

Abstract

This paper addresses the attitude tracking problem for small-scale unmanned helicopters under multisource disturbances. A composite dynamic gain control scheme is developed, integrating a disturbance observer with the fully actuated system approach. Unlike existing methods, the proposed approach explicitly considers both angular rate constraints and main rotor flapping dynamics, achieving high-precision attitude tracking without violating the rate limits. The results of a simulation based on a high-fidelity unmanned helicopter model demonstrate the effectiveness of the method.

Keywords: Unmanned helicopter, Disturbance observer, Angular rate constraint, Dynamic gain control, Fully actuated system approach

Citation: Kong Z, Li P, Li F, Zhao Z. 2026. Composite angular rate constrained control for unmanned helicopter attitude systems with consideration of flapping dynamics via a fully actuated system approach. *International Journal of Micro Air Vehicles* 18: e019 https://doi.org/10.48130/mav-0026-0022

Introduction

Unmanned helicopters (UHs) are rotor-wing aircraft characterized by high maneuverability and vertical take-off and landing capability, attracting extensive attention in both military and civilian domains[1]. For small-scale UHs that perform tasks such as reconnaissance and agricultural irrigation, precise tracking control is essential to ensure high performance[2]. The three-axis acceleration of an UH is primarily governed by the main rotor's lift through attitude variations. To accomplish complex tasks, UHs are required to perform agile maneuvers, which induce rapid attitude changes and consequently excite main rotor flapping dynamics. The attitude dynamics exhibit strong nonlinearity, coupling, and sensitivity to external gusts; internal parameter perturbations; and unmodeled dynamics[3], thereby posing significant challenges to the control system's design. Moreover, rapid attitude variations can compromise flights' stability and safety, necessitating explicit consideration of the angular rate constraints. Therefore, attitude controller designs that simultaneously account for main rotor flapping dynamics and state constraints, including angular rate limits, are critical for achieving safe and high-performance UH control[4].

To address multisource disturbances in the attitude loop of UHs, the disturbance observer-based control (DOBC) framework is widely used. The DOBC strategy estimates lumped disturbances via an observer and compensates for them in a feedforward manner, resulting in fast performance in disturbance rejection[5]. The modular nature of the DOBC strategy also facilitates integration with other control algorithms[5]. A nonlinear disturbance observer-based output boundary protection method has been proposed to handle external disturbances during UHs' trajectory tracking[6]. An adaptive smooth disturbance observer is integrated with a fast finite-time backstepping controller to achieve attitude tracking of a small UH that is subject to lumped disturbances[7]. Moreover, an online adaptive learning-based observer is designed to approximate the system's dynamic inversion for decoupling and is combined with a discrete-time model predictive controller to improve the system's stability and dynamic performance[8]. To counteract measurement noise and disturbances in the attitude systems of quadrotor unmanned aerial vehicles (UAVs), a combined observer based on a Kalman filter and a generalized proportional integral observer has been proposed, achieving high-precision attitude tracking with effective noise suppression[9]. Despite achieving fast and effective disturbance rejection, most existing DOBC methods do not adequately account for angular rate constraints.

To address state constraints in helicopters' flight control systems, various constrained output feedback control methods have been developed[10]. For instance, a robust multiple-state constrained control method has been designed for the position loop of a quadrotor to maintain its position and velocity within prescribed bounds[11]. A barrier Lyapunov function was used to enforce the attitude and flapping angle constraints, ensuring the boundedness of all closed-loop signals and maintaining tracking errors within prescribed performance bounds at all times[12]. To simultaneously address state constraints and input saturation, a reinforcement-learning-based robust tracking controller for UHs was introduced that incorporates a barrier function and an input-dependent nonquadratic term into the optimal control formulation[13]. Within the DOBC framework, a composite backstepping safety protection controller built on a second-order disturbance observer has been proposed to address attitude and flapping angle constraints while enhancing disturbance rejection performance[14].

To the best of our knowledge, existing DOBC methods for UHs, though capable of handling constraints and providing fast disturbance rejection, typically rely on conventional state-space models that often result in structurally complex controllers. As a promising alternative, the fully actuated system approach (FASA) has recently been proposed to simplify controller design by canceling nonlinearity in the system and rearranging the dynamics[15]. FASA has demonstrated its effectiveness in flight control applications, including for

© The Author(s)

https://doi.org/10.48130/mav-0026-0022

UAVs[16] and spacecraft systems[17]. Given that the UH is a high-order, underactuated, and strongly nonlinear system, the extension of FASA to UH flight control presents a meaningful and open research problem.

Aiming at the attitude control of UHs with constraint of the angular rate under disturbance, a composite dynamic gain control scheme based on a disturbance observer and FASA is proposed. First, the finite-time disturbance observer is introduced to estimate the lumped disturbance in the fully actuated attitude error dynamics. Next, the extended state observer is introduced to estimate the torque of the UH on the basis of the flapping dynamics of the main rotor. Finally, by using the FASA, a composite dynamic gain control scheme based on the estimation's information is constructed. The main contribution of this paper are summarized as follows: (1) High-precision attitude tracking without violating angular rate constraints under varying disturbances; (2) smooth actual control action through torque loop feedback control based on the estimated states; and (3) effective disturbance rejection and robustness via feedforward compensation of the estimated disturbances.

Modeling and problem formulation

Modeling of the small-scale UH system

Under the assumption that the UH is a rigid body, its attitude dynamics can be described as follows[18]:

$$\begin{cases} \dot{\boldsymbol{\Theta}} = \boldsymbol{T}(\boldsymbol{\Theta})\boldsymbol{\Omega}, \\ \dot{\boldsymbol{\Omega}} = \mathbf{J}^{-1}(-\boldsymbol{\Omega}\times\mathbf{J}\boldsymbol{\Omega}+\boldsymbol{\Gamma}) + \boldsymbol{D}_{\boldsymbol{\Omega}}, \end{cases} \tag{1}$$

where $\boldsymbol{\Theta} = [\phi, \theta, \psi]^{\mathbf{T}}$ is the attitude angle of the helicopter; ϕ, θ, ψ are the roll angle, pitch angle, and yaw angle, respectively; $\boldsymbol{\Omega} = [p, q, r]^T$ are the angular rates; p, q, r are the angular rate or roll, pitch, and yaw, respectively; $\mathbf{J} = \mathrm{diag}\{I_x, I_y, I_z\}$ is the inertia matrix; $\boldsymbol{\Gamma} = [L, M, N]^T$; L, M, N are the roll moment, pitch moment, and yaw moment, respectively; $\boldsymbol{D}_{\boldsymbol{\Omega}} = [D_p, D_q, D_r]^T$ are disturbed moments and; $\boldsymbol{T}(\boldsymbol{\Theta})$ is the rotation matrix and has the following form:

$$\boldsymbol{T}(\boldsymbol{\Theta}) = \begin{bmatrix} 1 & s\phi t\theta & c\phi t\theta \\ 0 & c\phi & s\phi \\ 0 & s\phi/c\theta & c\phi/c\theta \end{bmatrix},$$

where $c\phi = \cos\phi, s\phi = \sin\phi, c\theta = \cos\theta$, and $t\theta = \tan\theta$.

The yaw moment N is determined by the angular rate of yaw r, the collective pitch input δ_{col}, and the input of the tail rotor δ_{ped}

$$N = N_r r + N_{col}\delta_{col} + N_{ped}\delta_{ped}. \tag{2}$$

where N_r, N_{col}, and N_{ped} are constant coefficients. The roll moment L and pitch moment M are determined by the flapping angles

$$\begin{bmatrix} L \\ M \end{bmatrix} = \begin{bmatrix} L_a & L_b \\ M_a & M_b \end{bmatrix}\begin{bmatrix} a \\ b \end{bmatrix}, \tag{3}$$

where a and b are flapping angles used to depict the flapping of the main rotor along the longitudinal and lateral axis, respectively; and L_a, M_b, L_b, and M_a are constant coefficients. The dynamics of the flapping angles are described as follows[12]:

$$\begin{bmatrix} \dot{a} \\ \dot{b} \end{bmatrix} = \begin{bmatrix} c & A_b \\ B_a & c \end{bmatrix}\begin{bmatrix} a \\ b \end{bmatrix} + \begin{bmatrix} 0 & -1 \\ -1 & 0 \end{bmatrix}\begin{bmatrix} p \\ q \end{bmatrix} + \begin{bmatrix} A_{lon} & A_{lat} \\ B_{lon} & B_{lat} \end{bmatrix}\begin{bmatrix} \delta_{lon} \\ \delta_{lat} \end{bmatrix}, \tag{4}$$

where c, A_b, B_a, A_{lon}, A_{lat}, B_{lon}, and B_{lat} are the parameters determined by the mechanical structure of the helicopter and δ_{lon}, δ_{lat} are the lateral and longitudinal cyclic inputs, respectively.

The altitude translational dynamics of the helicopter can be described by the following standard force balance model[19]:

$$m\ddot{h} = -mg + T\cos\phi\cos\theta, \tag{5}$$

where g is the gravity coefficient, h is the altitude of the helicopter, and T is the main rotor thrust which is determined by collective pitch input δ_{col}:

$$T = T_0 + Z_{col}\delta_{col}, \tag{6}$$

where Z_{col} are constant parameters and $T_0 = mg$.

Problem formulation

Define the attitude tracking error of the helicopter as

$$\boldsymbol{e}_{\boldsymbol{\Theta}} = \boldsymbol{\Theta} - \boldsymbol{\Theta}_{\boldsymbol{r}} = [e_\phi, e_\theta, e_\psi]^T = [\phi - \phi_r, \theta - \theta_r, \psi - \psi_r]^T,$$

where $\boldsymbol{\Theta}_{\boldsymbol{r}} = [\phi_r, \theta_r, \psi_r]^T$ and ϕ_r, θ_r, ψ_r are attitude references. The attitude tracking error dynamics can be obtained by Eq. (1) as follows:

$$\ddot{\boldsymbol{e}}_{\boldsymbol{\Theta}} = \boldsymbol{T}(\boldsymbol{\Theta})(-\mathbf{J}^{-1}\boldsymbol{\Omega}\times\mathbf{J}\boldsymbol{\Omega} + \mathbf{J}^{-1}\boldsymbol{\Gamma}) + \dot{\boldsymbol{T}}(\boldsymbol{\Theta})\boldsymbol{\Omega} + \boldsymbol{D}_{\boldsymbol{LA}}, \tag{7}$$

with

$$\dot{\boldsymbol{T}}(\boldsymbol{\Theta}) = \begin{bmatrix} 0 & \frac{\dot{\theta}s\phi}{c^2\theta} + \dot{\phi}c\phi t\theta & -\dot{\phi}s\phi t\theta + \frac{\dot{\theta}c\phi}{c^2\theta} \\ 0 & -\dot{\phi}s\phi & \dot{\phi}c\phi \\ 0 & \frac{\dot{\phi}\cdot c\phi}{c\theta} + \frac{\dot{\theta}s\phi t\theta}{c\theta} & \frac{-\dot{\phi}s\phi}{c\theta} + \frac{\dot{\theta}c\phi t\theta}{c\theta} \end{bmatrix}, \quad \boldsymbol{D}_{\boldsymbol{LA}} = \boldsymbol{T}(\boldsymbol{\Theta})\boldsymbol{D}_{\boldsymbol{\Omega}} - \ddot{\boldsymbol{\Theta}}_{\boldsymbol{r}},$$

where $\dot{\boldsymbol{T}}(\boldsymbol{\Theta})$ is the derivative of $\boldsymbol{T}(\boldsymbol{\Theta})$, $\boldsymbol{D}_{\boldsymbol{LA}}$ is the lumped disturbances, and $\ddot{\boldsymbol{\Theta}}_{\boldsymbol{r}} = [\ddot{\phi}_r, \ddot{\theta}_r, \ddot{\psi}_r]^T$ is the second-order derivative of the attitude angle reference.

Introduce the following definition:

$$\begin{bmatrix} \tau_1 \\ \tau_2 \\ \tau_3 \end{bmatrix} = \boldsymbol{T}(\boldsymbol{\Theta})\mathbf{J}^{-1}\boldsymbol{\Gamma}, \quad \begin{bmatrix} D_\phi \\ D_\theta \\ D_\psi \end{bmatrix} = \boldsymbol{D}_{\boldsymbol{LA}},$$
$$\begin{bmatrix} f_1 \\ f_2 \\ f_3 \end{bmatrix} = -\boldsymbol{T}(\boldsymbol{\Theta})(\mathbf{J}^{-1}\boldsymbol{\Omega}\times\mathbf{J}\boldsymbol{\Omega}) + \dot{\boldsymbol{T}}(\boldsymbol{\Theta})\boldsymbol{\Omega}. \tag{8}$$

If we substitute Eq. (8) into Eq. (7), the following fully actuated attitude error dynamic is introduced as

$$\begin{cases} \ddot{e}_\phi = \tau_1 + f_1 + D_\phi, \\ \ddot{e}_\theta = \tau_2 + f_2 + D_\theta, \\ \ddot{e}_\psi = \tau_3 + f_3 + D_\psi. \end{cases} \tag{9}$$

To ensure the safety of the UH, the angular rate are usually required to operate between a certain range. As a result, the angular rate of the attitude angle is considered in this study, which is are required to satisfy $m_{\phi 1} < \dot{\phi} < m_{\phi 2}$, $m_{\theta 1} < \dot{\theta} < m_{\theta 2}$, and $m_{\psi 1} < \dot{\psi} < m_{\psi 2}$, where $\dot{\phi}$, $\dot{\theta}$, $\dot{\psi}$ are the rate of change in the roll, pitch, and yaw angles, respectively; $m_{\phi 1}$, $m_{\phi 2}$, $m_{\theta 1}$, $m_{\theta 2}$, $m_{\psi 1}$, and $m_{\psi 2}$ are known constants with $m_{\phi 1} < 0 < m_{\phi 2}$, $m_{\theta 1} < 0 < m_{\theta 2}$, $m_{\psi 1} < 0 < m_{\psi 2}$.

We can conclude from the description above that the internal signal flow of the helicopter's attitude torque subsystem behaves as shown in Fig. 1, and both the attitude controller and the torque controller need to be designed for the attitude control system when the flapping dynamics are considered.

Design of the composite controller

Design of the disturbance observers in the attitude loop

Assumption 1. The lumped disturbances D_ϕ, D_θ, *and* D_ψ in Eq. (9) are differentiable and satisfy

$$|\dot{D}_\phi| \leqslant l_1, \ |\dot{D}_\theta| \leqslant l_2, \ |\dot{D}_\psi| \leqslant l_3,$$

where l_1, l_2, and l_3 are positive known constants.

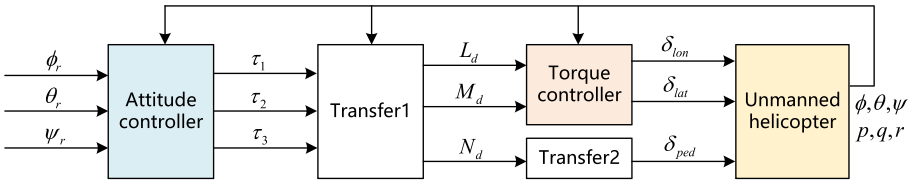

Fig. 1 Simplified control structure for the UH attitude system.

In order to estimate the lumped disturbances D_ϕ, D_θ, and D_ψ in the fully actuated attitude error dynamics, the finite-time disturbance observers (FTDOs) are designed as follows:

$$\begin{cases} \dot{z}_{11} = v_{11}, \\ \dot{z}_{12} = \tau_1 + f_1 + v_{12}, \\ \dot{z}_{13} = -1.1 l_{Ao1}\text{sign}(z_{13} - v_{12}), \\ v_{11} = -3 l_{Ao1}^{1/3}|z_{11} - e_\phi|^{2/3}\text{sign}(z_{11} - e_\phi) + z_{12}, \\ v_{12} = -1.5 l_{Ao1}^{1/2}|z_{12} - v_{11}|^{1/2}\text{sign}(z_{12} - v_{11}) + z_{13}, \\ \hat{D}_\phi = z_{13}, \ \hat{e}_\phi = z_{12}, \end{cases} \tag{10}$$

$$\begin{cases} \dot{z}_{21} = v_{21}, \\ \dot{z}_{22} = \tau_2 + f_2 + v_{22}, \\ \dot{z}_{23} = -1.1 l_{Ao2}\text{sign}(z_{23} - v_{22}), \\ v_{21} = -3 l_{Ao2}^{1/3}|z_{21} - e_\theta|^{2/3}\text{sign}(z_{21} - e_\theta) + z_{22}, \\ v_{22} = -1.5 l_{Ao2}^{1/2}|z_{22} - v_{21}|^{1/2}\text{sign}(z_{22} - v_{21}) + z_{23}, \\ \hat{D}_\theta = z_{23}, \ \hat{e}_\theta = z_{22}, \end{cases} \tag{11}$$

$$\begin{cases} \dot{z}_{31} = v_{31}, \\ \dot{z}_{32} = \tau_3 + f_3 + v_{32}, \\ \dot{z}_{33} = -1.1 l_{Ao3}\text{sign}(z_{33} - v_{32}), \\ v_{31} = -3 l_{Ao3}^{1/3}|z_{31} - e_\psi|^{2/3}\text{sign}(z_{31} - e_\psi) + z_{32}, \\ v_{32} = -1.5 l_{Ao3}^{1/2}|z_{32} - v_{31}|^{1/2}\text{sign}(z_{32} - v_{31}) + z_{33}, \\ \hat{D}_\psi = z_{33}, \ \hat{e}_\psi = z_{32}, \end{cases} \tag{12}$$

where l_{Ao1}, l_{Ao2}, and l_{Ao3} are the observer gains and they are constants which satisfy $l_{Ao1} > l_1, \ l_{Ao2} > l_2, and \ l_{Ao3} > l_3$.

Define the estimation errors of observers in (10)–(12) as

$$\begin{aligned} &e_{A1} = \hat{e}_\phi - \dot{e}_\phi, \ e_{A2} = \hat{e}_\theta - \dot{e}_\theta, \ e_{A3} = \hat{e}_\psi - \dot{e}_\psi, \\ &e_{D1} = \hat{D}_\phi - D_\phi, \ e_{D2} = \hat{D}_\theta - D_\theta, \ e_{D3} = \hat{D}_\psi - D_\psi, \end{aligned} \tag{13}$$

where $\hat{\dot{e}}_\phi, \hat{\dot{e}}_\theta, \hat{\dot{e}}_\psi$ are the estimations of $\dot{e}_\phi, \dot{e}_\theta, \dot{e}_\psi$; and $\hat{D}_\phi, \hat{D}_\theta, \hat{D}_\psi$ are the estimations of lumped disturbances D_ϕ, D_θ, D_ψ. Considering Assumption 1 and the observer gains conditions $l_{Ao1} > l_1$, $l_{Ao2} > l_2$, $l_{Ao3} > l_3$, the estimation errors, i.e., e_{A1}, e_{A2}, e_{A3} and e_{D1}, e_{D2}, e_{D3} in Eq. (13), converge to zero in finite time[20].

Design of the torque filter in the torque loop

It can be observed from Eq. (3) that the roll and pitch moments L and M are determined by the flapping angles, whereas the flapping angles can not be measured directly in practical engineering. Therefore, we need to design observers to estimate the dynamics of the torque.

Combining Eq.(3) and (4) yields

$$\dot{\boldsymbol{\tau}}_2 = \boldsymbol{\Phi}\mathbf{A_1}\boldsymbol{\Phi}^{-1}\boldsymbol{\tau}_2 + \boldsymbol{\Phi}\mathbf{A}\boldsymbol{\omega}_2 + \boldsymbol{u}_2, \tag{14}$$

with

$$\boldsymbol{\omega}_2 = \begin{bmatrix} p \\ q \end{bmatrix}, \ \boldsymbol{\tau}_2 = \begin{bmatrix} L \\ M \end{bmatrix},$$
$$\boldsymbol{u}_2 = \begin{bmatrix} L_a(A_{lon}\delta_{lon} + A_{lat}\delta_{lat}) + L_b(B_{lon}\delta_{lon} + B_{lat}\delta_{lat}) \\ M_a(A_{lon}\delta_{lon} + A_{lat}\delta_{lat}) + M_b(B_{lon}\delta_{lon} + B_{lat}\delta_{lat}) \end{bmatrix}.$$

The parameter matrix is

$$\boldsymbol{\Phi} = \begin{bmatrix} L_a & L_b \\ M_a & M_b \end{bmatrix}, \ \mathbf{A_1} = \begin{bmatrix} c & A_b \\ B_a & c \end{bmatrix}, \ \mathbf{A} = \begin{bmatrix} 0 & -1 \\ -1 & 0 \end{bmatrix}.$$

Taking the frequency transformation of Eq. (14) yields:

$$s\boldsymbol{\tau}_2(s) = \boldsymbol{\Phi}\mathbf{A_1}\boldsymbol{\Phi}^{-1}\boldsymbol{\tau}_2(s) + \boldsymbol{\Phi}\mathbf{A}\boldsymbol{\omega}_2(s) + \boldsymbol{u}_2(s), \tag{15}$$

and it shows

$$\boldsymbol{\tau}_2(s) = (s\mathbf{I} - \boldsymbol{\Phi}\mathbf{A_1}\boldsymbol{\Phi}^{-1})^{-1}(\boldsymbol{\Phi}\mathbf{A}\boldsymbol{\omega}_2(s) + \boldsymbol{u}_2(s)). \tag{16}$$

Define:

$$\frac{\boldsymbol{N}(s)}{\boldsymbol{M}(s)} = (s\mathbf{I} - \boldsymbol{\Phi}\mathbf{A_1}\boldsymbol{\Phi}^{-1})^{-1}, \ \boldsymbol{N_1}(s) = \boldsymbol{N}(s)\boldsymbol{\Phi}\mathbf{A}. \tag{17}$$

We then obtain the following from Eq. (16):

$$\boldsymbol{\tau}_2(s) = \frac{\boldsymbol{N_1}(s)}{\boldsymbol{M}(s)}\boldsymbol{\omega}_2(s) + \frac{\boldsymbol{N}(s)}{\boldsymbol{M}(s)}\boldsymbol{u}_2(s). \tag{18}$$

As $\boldsymbol{\omega}_2(s)$ and $\boldsymbol{u}_2(s)$ is known, and hence $\boldsymbol{\tau}_2(s)$ can be obtained from $\boldsymbol{\omega}_2(s)$ and $\boldsymbol{u}_2(s)$. $\hat{\boldsymbol{\tau}}_2(t)$ can be obtained by taking the inverse frequency domain transformation of $\boldsymbol{\tau}_2(s)$, the initial state of $\hat{\boldsymbol{\tau}}_2(t)$ and $\boldsymbol{\tau}_2(t)$ are different and they gradually become the same over time. Define the filter estimation error

$$\boldsymbol{\delta}^f_{\tau_2} = \hat{\boldsymbol{\tau}}_2(t) - \boldsymbol{\tau}_2(t), \tag{19}$$

To provide an explicit convergence analysis, write $\boldsymbol{A}_f = \boldsymbol{\Phi}\boldsymbol{A_1}\boldsymbol{\Phi}^{-1}$. Under the nominal model, the torque filter and the actual torque dynamics share the same input terms $\boldsymbol{\Phi}\boldsymbol{A}\omega_2 + \boldsymbol{u}_2$, and therefore

$$\dot{\boldsymbol{\delta}}^f_{\tau_2} = \boldsymbol{A}_f\boldsymbol{\delta}^f_{\tau_2}. \tag{20}$$

Since $\boldsymbol{A}_f$ is similar to $\boldsymbol{A}_1$, its eigenvalues are

$$\lambda_{1,2} = c \pm \sqrt{A_b B_a}. \tag{21}$$

For the identified helicopter parameters used in this study, $c < 0$ and $c^2 > A_b B_a$, which implies that $\boldsymbol{A}_f$ is Hurwitz. Hence, the nominal linear error system in Eq. (20) is exponentially stable, and $\boldsymbol{\delta}^f_{\tau_2}$ converges to zero under nominal conditions. In practical implementation, parameter mismatch, measurement noise, and discretization residuals can be collected into a bounded perturbation $\boldsymbol{\eta}(t)$. The corresponding perturbed filter-error dynamics can be written as

$$\dot{\boldsymbol{\delta}}^f_{\tau_2} = \boldsymbol{A}_f\boldsymbol{\delta}^f_{\tau_2} + \boldsymbol{\eta}(t). \tag{22}$$

Under the standard operating condition that the torque, angular-rate, and control input signals remain bounded, the perturbation term is bounded, namely $\|\boldsymbol{\eta}(t)\| \le \bar{\eta}$. Since $\boldsymbol{A}_f$ is Hurwitz, Eq. (22) is a stable finite-dimensional linear time-invariant system. According to the bounded-input–bounded-output stability theorem, the bounded input $\boldsymbol{\eta}(t)$ produces a bounded output $\boldsymbol{\delta}^f_{\tau_2}(t)$. Therefore, the torque filter estimation error is bounded and converges to a small neighborhood of zero under practical perturbations. When $\bar{\eta} = 0$, Eq. (22) reduces to the nominal case in Eq. (20), and the estimation error converges to zero asymptotically.

Design of the composite dynamic gain attitude controller

Theorem 1. For the fully actuated attitude error dynamic in Eq. (9), if Assumption 1 holds and the initial value of attitude angle rates

https://doi.org/10.48130/mav-0026-0022

satisfy $\dot{\phi}(0) \in (m_{\phi 1}, m_{\phi 2})$, $\dot{\theta}(0) \in (m_{\theta 1}, m_{\theta 2})$, $\dot{\psi}(0) \in (m_{\psi 1}, m_{\psi 2})$, the following FASA-based composite dynamic gain attitude controller is

$$\begin{cases} \tau_1 = -f_1 - \hat{D}_\phi - k_{\phi 1} e_\phi - [k_{\phi 2} + \dfrac{l_\phi}{(m_{\phi 2} - \dot{e}_\phi)(\dot{e}_\phi - m_{\phi 1})}]\dot{e}_\phi, \\ \tau_2 = -f_2 - \hat{D}_\theta - k_{\theta 1} e_\theta - [k_{\theta 2} + \dfrac{l_\theta}{(m_{\theta 2} - \dot{e}_\theta)(\dot{e}_\theta - m_{\theta 1})}]\dot{e}_\theta, \\ \tau_3 = -f_3 - \hat{D}_\psi - k_{\psi 1} e_\psi - [k_{\psi 2} + \dfrac{l_\psi}{(m_{\psi 2} - \dot{e}_\psi)(\dot{e}_\psi - m_{\psi 1})}]\dot{e}_\psi, \end{cases} \tag{23}$$

where $k_{\phi 1}$, $k_{\phi 2}$, $k_{\theta 1}$, $k_{\theta 2}$, $k_{\psi 1}$, $k_{\psi 2}$, l_ϕ, l_θ, l_ψ are positive controller gains which guarantee that the attitude tracking errors e_ϕ, e_θ, e_ψ converge to zero asymptotically and also guarantee that the attitude angular rates satisfy $\dot{\phi} \in (m_{\phi 1}, m_{\phi 2})$, $\dot{\theta} \in (m_{\theta 1}, m_{\theta 2})$, *and* $\dot{\psi} \in (m_{\psi 1}, m_{\psi 2})$; and $\hat{D}_\phi$, $\hat{D}_\theta$, $\hat{D}_\psi$ are obtained by the observers in Eqs (10)–(12). Since the attitude commands ϕ_r, θ_r, ψ_r are constant in the regulation problem considered in this study, we have $\dot{\phi}_r = \dot{\theta}_r = \dot{\psi}_r = 0$, and thus the angular rate constraints are equivalent to the constraints on the tracking error derivatives.

Equation (8) implies that the virtual torques τ_1, τ_2, τ_3 are determined by the real torques L, M, N and the corresponding desired torques for attitude controller (Eq. [23]) can be calculated as

$$\begin{bmatrix} L_d \\ M_d \\ N_d \end{bmatrix} = \mathbf{J}\boldsymbol{T}(\boldsymbol{\Theta})^{-1} \begin{bmatrix} \tau_1 \\ \tau_2 \\ \tau_3 \end{bmatrix}, \tag{24}$$

where L_d, M_d, *and* N_d are corresponding desired torques for attitude controller.

Remark 1. The parameters l_ϕ, l_θ, and l_ψ determine the activation strength of the barrier-type damping terms in the proposed attitude loop controller. Since these three parameters enter the controller through the same structure, the roll channel is taken as an example. Here, l_ϕ appears in the additive barrier gain, which increases rapidly as $\dot{e}_\phi$ approaches either constraint boundary. A larger l_ϕ strengthens the boundary repulsion and improves rate-constraint enforcement, but an excessively large value introduces strong damping and slows the transient response. Conversely, a smaller l_ϕ reduces conservatism and may accelerate the response in the normal operating region, but it weakens the protection near the rate boundary and may cause larger overshoot. Therefore, l_ϕ, l_θ, and l_ψ should be selected to balance constraint enforcement and transient tracking performance. In this study, $l_\phi = l_\theta = 3$ and $l_\psi = 2$ are adopted for the Raptor-90 helicopter.

Design of the composite torque loop controller

Define the torque tracking error in the roll and pitch channels as follows:

$$\boldsymbol{e}_{\boldsymbol{\tau}_2} = [L - L_d, M - M_d]^T.$$

Tracking error dynamic can be obtained by Eq. (14) as follows:

$$\dot{\boldsymbol{e}}_{\boldsymbol{\tau}_2} = \dot{\boldsymbol{\tau}}_2 - \dot{\boldsymbol{\tau}}_2^{\boldsymbol{d}} = \boldsymbol{\Phi} \boldsymbol{A}_1 \boldsymbol{\Phi}^{-1} \boldsymbol{\tau}_2 + \boldsymbol{\Phi} \mathbf{A} \boldsymbol{\omega}_2 + \boldsymbol{u}_2 - \dot{\boldsymbol{\tau}}_2^{\boldsymbol{d}}, \tag{25}$$

where $\boldsymbol{\tau}_2^{\boldsymbol{d}} = [L_d, M_d]^T$, $\dot{\boldsymbol{\tau}}_2^{\boldsymbol{d}} = [\dot{L}_d, \dot{M}_d]^T$. In order to estimate $\dot{L}_d$, $\dot{M}_d$, the tracking differentiator[21] is introduced. Given that the tracking differentiator formulas are symmetrical in the roll and pitch channels, the roll channel is introduced as an example.

$$\begin{cases} \dot{\eta}_1 = \eta_2, \\ \dot{\eta}_2 = fhan(\eta_1, \eta_2, L, s, h), \end{cases} \quad fhan(\eta_1, \eta_2, L, s, h) = \begin{cases} -s\mathrm{sgn}(n), & |n| > m, \\ -s\dfrac{n}{m}, & |n| \leqslant m, \end{cases} \tag{26}$$

where η_1, η_2 are the estimation of L_d and its derivative $\dot{L}_d$; h and s are positive constants; and m, n are calculated as

$$m = sh, \quad y = \eta_1 - L_d + h\eta_2,$$

$$n = \begin{cases} \eta_2 + (\sqrt{m^2 + 8s|y|} - m)\dfrac{\mathrm{sgn}(y)}{2}, & |y| > m, \\ \eta_2 + \dfrac{y}{h}, & |y| \leqslant m. \end{cases}$$

Theorem 2. For the torque tracking error dynamic (Eq. [25]), the following composite torque loop controller:

$$\boldsymbol{u}_2 = -\boldsymbol{\Phi} \mathbf{A}_1 \boldsymbol{\Phi}^{-1} \hat{\boldsymbol{\tau}}_2 - \boldsymbol{\Phi} \mathbf{A} \boldsymbol{\omega}_2 + \widehat{\dot{\boldsymbol{\tau}}_2^{\boldsymbol{d}}} - \boldsymbol{k}_\tau (\hat{\boldsymbol{\tau}}_2 - \boldsymbol{\tau}_2^{\boldsymbol{d}}), \tag{27}$$

Guarantees that the torque tracking errors converge to zero asymptotically, where $\boldsymbol{k}_\tau = [k_L, k_M]^T$ and k_L, k_M are positive constants, $\hat{\boldsymbol{\tau}}_2$ is the estimation of the roll and pitch torque achieved by the torque filter (Eq. [16]); and $\widehat{\dot{\boldsymbol{\tau}}_2^{\boldsymbol{d}}} = [\hat{\dot{L}}_d, \hat{\dot{M}}_d]^T$ are the estimation of desired torque derivatives which are obtained by the tracking differentiator (Eq. [26]).

Derivation of real control action

The cyclic control input is calculated as follows:

$$\begin{bmatrix} \delta_{lon} \\ \delta_{lat} \end{bmatrix} = \begin{bmatrix} A_{lon} & A_{lat} \\ B_{lon} & B_{lat} \end{bmatrix}^{-1} \begin{bmatrix} L_a & L_b \\ M_a & M_b \end{bmatrix}^{-1} \boldsymbol{u}_2, \tag{28}$$

where $\boldsymbol{u}_2$ is from Eq. (27). The collective pitch input δ_{col} is assumed to balance the weight of helicopter, and it can be calculated via Eq. (6) as follows:

$$\delta_{col} = \frac{1}{Z_{col}} \left(1 - \frac{1}{\cos\phi \cos\theta}\right) mg. \tag{29}$$

The input of the tail rotor can be calculated based on Eq. (2) as follows:

$$\delta_{ped} = (N_d - N_r r - N_{col}\delta_{col})/N_{ped}, \tag{30}$$

where N_d is from Eq. (8), and δ_{col} is from Eq. (29).

Figure 2 presents the control structure of the proposed composite dynamic gain controller for the UH attitude system.

Stability analysis

Analysis in the attitude control loop

It can be observed from Eq. (9) and Eq. (23) that both the attitude dynamics and the controllers in the roll, pitch and yaw channels are symmetrical. Hence it is only necessary to prove the stability in one channel; the others can be deduced similarly. Without loss of generality, we choose the roll angle as an example to prove the stability of the attitude controller.

Define a Lyapunov function in terms of the roll angle tracking error e_ϕ as

$$V_1 = \frac{1}{2} k_{\phi 1} e_\phi^2 + \frac{1}{2} \dot{e}_\phi^2.$$

Substituting the controller (Eq. [23]) into the attitude dynamics equation (Eq. [9]) yields the closed-loop tracking error dynamics of the roll angle

$$\ddot{e}_\phi = -k_{\phi 1} e_\phi - \left[k_{\phi 2} + \frac{l_\phi}{(m_{\phi 2} - \dot{e}_\phi)(\dot{e}_\phi - m_{\phi 1})}\right] \dot{e}_\phi - e_{D1}. \tag{31}$$

Taking the derivative of V_1 along Eq. (31) yields

$$\dot{V}_1 = -\left[k_{\phi 2} + \frac{l_\phi}{(m_{\phi 2} - \dot{e}_\phi)(\dot{e}_\phi - m_{\phi 1})}\right] \dot{e}_\phi^2 - \dot{e}_\phi e_{D1}, \tag{32}$$

To further quantify the influence of the observer's estimation error before finite-time convergence, denote

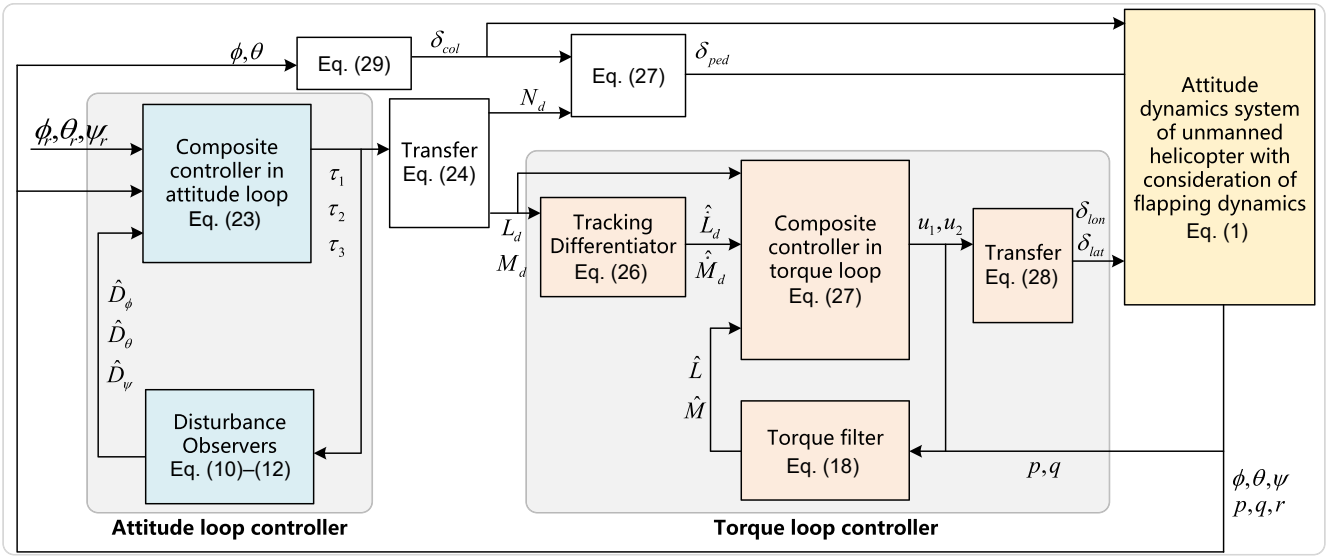

Fig. 2 Control structure of the proposed composite dynamic gain controller for the UH attitude system.

$$B(\dot{e}_\phi)=\frac{l_\phi}{(m_{\phi 2}-\dot{e}_\phi)(\dot{e}_\phi-m_{\phi 1})}. \tag{33}$$

Since $(m_{\phi 2}-\dot{e}_\phi)(\dot{e}_\phi-m_{\phi 1})\leqslant(m_{\phi 2}-m_{\phi 1})^2/4$ for $\dot{e}_\phi\in(m_{\phi 1},m_{\phi 2})$, one has

$$B(\dot{e}_\phi)\geqslant B_{\min}=\frac{4l_\phi}{(m_{\phi 2}-m_{\phi 1})^2}>0. \tag{34}$$

Using Young's inequality, the Lyapunov derivative satisfies

$$\dot{V}_1\leqslant-\left(k_{\phi 2}+\frac{B_{\min}}{2}\right)\dot{e}_\phi^2+\frac{1}{2B_{\min}}e_{D1}^2. \tag{35}$$

The finite-time disturbance observer ensures that e_{D1} is bounded before its convergence and satisfies $e_{D1}(t)=0$ for $t\geqslant T_1$. Let $|e_{D1}(t)|\leqslant\bar{e}_{D1}$ for $0\leqslant t<T_1$. Then we have

$$V_1(t)\leqslant V_1(0)+\frac{\bar{e}_{D1}^2}{2B_{\min}}T_1,\quad 0\leqslant t<T_1, \tag{36}$$

which proves that e_ϕ and $\dot{e}_\phi$ remain uniformly bounded during the observer transient. After T_1, the estimation error vanishes and $\dot{V}_1\leqslant-[k_{\phi 2}+B(\dot{e}_\phi)]\dot{e}_\phi^2\leqslant 0$. Since the prescribed interval contains the origin, i.e., $m_{\phi 1}<0<m_{\phi 2}$, and $B(0)$ is well defined and positive. Around the equilibrium, the local linearized dynamics are characterized by

$$s^2+[k_{\phi 2}+B(0)]s+k_{\phi 1}=0, \tag{37}$$

whose roots have negative real parts. Therefore, the post-transient response is locally exponentially convergent, and its local linearized decay rate can be characterized by $\alpha_{\text{loc}}=-\max_i\Re(s_i)>0$, where s_i are the roots of the characteristic equation. The pitch and yaw channels can be analyzed in the same way.

Considering $\dot{\phi}(0)\in(m_{\phi 1},m_{\phi 2})$ and the command of attitude angles are constant, we have $[m_{\phi 2}-\dot{e}_\phi(0)][\dot{e}_\phi(0)-m_{\phi 1}]>0$. After the observer error vanishes, it follows from the post-transient inequality $\dot{V}_1\leqslant-[k_{\phi 2}+B(\dot{e}_\phi)]\dot{e}_\phi^2\leqslant 0$ that V_1 is nonincreasing. If we define $M(\dot{e}_\phi)=(m_{\phi 2}-\dot{e}_\phi)(\dot{e}_\phi-m_{\phi 1})$, we can analyze the dynamics of $\dot{e}_\phi$ in the following three cases.

Case I $\dot{e}_\phi(t)\in(m_{\phi 1},m_{\phi 2})$: In this case, $M(\dot{e}_\phi)>0$ and we have $\dot{V}_1<-k_{\phi 2}\dot{e}_\phi^2\leqslant 0$. This indicates that e_ϕ will converge to zero monotonically.

Case II $\dot{e}_\phi(t)\to m_{\phi 1}$: In this case, $M(\dot{e}_\phi)\to 0^+$, $l_\phi/M(\dot{e}_\phi)\to+\infty$. Considering $m_{\phi 1}<0$, it can be deduced that $\dot{e}_\phi(t)<0$ when $\dot{e}_\phi(t)$ approaches $m_{\phi 1}$. Therefore, it can be obtained from Eq. (31) that $\ddot{e}_\phi\to+\infty$ in this case, and it shows that $\dot{e}_\phi$ increases dramatically when $\dot{e}_\phi$ approaches $m_{\phi 1}$. Therefore, we have the conclusion that when $\dot{e}_\phi(t)\to m_{\phi 1}$, and once $\dot{e}_\phi$ increases, it will deviate from $m_{\phi 1}$ and converge to the bound $(m_{\phi 1},m_{\phi 2})$.

Case III $\dot{e}_\phi(t)\to m_{\phi 2}$: In this case, since $m_{\phi 2}>0,\dot{e}_\phi$ approaches $m_{\phi 2}$, this indicates that $\dot{e}_\phi$ increases and $\dot{e}_\phi>0$. When $\dot{e}_\phi(t)\to m_{\phi 2}$, $M(\dot{e}_\phi)\to 0^+$, and $l_\phi/M(\dot{e}_\phi)\to+\infty$, so it can be obtained from Eq. (31) that $\ddot{e}_\phi\to-\infty$. This indicates that $\dot{e}_\phi(t)$ will decrease dramatically when $\dot{e}_\phi$ approaches $m_{\phi 2}$, and then it will deviate from $m_{\phi 2}$ and converge to the bound $(m_{\phi 1},m_{\phi 2})$.

Therefore, we can conclude from Case II and Case III that $\dot{e}_\phi(t)$ will not escape the region $(m_{\phi 1},m_{\phi 2})$ once it is in that region. Considering that $\dot{\phi}(0)$ is in the region $(m_{\phi 1},m_{\phi 2})$, we conclude that $\dot{e}_\phi(t)$ will stay in $(m_{\phi 1},m_{\phi 2})$. It can be concluded from Case I that, e_ϕ will converge to zero asymptotically.

Analysis of the torque control loop

Define the estimation error of the demanded torques' derivative as

$$\boldsymbol{\delta}_{\tau_2}^d=\dot{\boldsymbol{\tau}}_2^d-\widehat{\dot{\boldsymbol{\tau}}_2^d}.$$

Substituting the torque controller Eq. (27) into Eq. (25) yields:

$$\dot{\boldsymbol{e}}_{\tau_2}=-\boldsymbol{k}_\tau\boldsymbol{e}_{\tau_2}+[\boldsymbol{\delta}_{\tau_2}^d-(\mathbf{A}_1+\boldsymbol{k}_\tau)\boldsymbol{\delta}_{\tau_2}^f].$$

As $\boldsymbol{k}_\tau$ is a positive symmetric matrix, it follows that $\dot{\boldsymbol{e}}_{\tau_2}=-\boldsymbol{k}_\tau\boldsymbol{e}_{\tau_2}$ converges to zero asymptotically. Considering that the torque estimation error $\boldsymbol{\delta}_{\tau_2}^f$ and the differentiator error $\boldsymbol{\delta}_{\tau_2}^d$ converge to bounded regions, the lumped term $\boldsymbol{M}=\boldsymbol{\delta}_{\tau_2}^d-(\mathbf{A}_1+\boldsymbol{k}_\tau)\boldsymbol{\delta}_{\tau_2}^f$ also converges to a bounded region. Therefore, on the basis of the bounded input bounded output (BIBO) theorem, we conclude that $\boldsymbol{e}_{\tau_2}$ converges to a bounded neighborhood close to zero[22].

Simulation analysis

Simulation setting

Simulations based on a small-scale UH are carried out in this part to verify the effectiveness of the proposed methods. The model

https://doi.org/10.48130/mav-0026-0022

parameters in the simulations are chosen based on a Raptor-90 helicopter and set as Table 1.

The parameters listed in Table 1 are used as the nominal model parameters for the controller design, and the superscript N indicates when parameter perturbations are considered. In the robustness simulation with inertia uncertainties, the actual moments of inertia of the simulated helicopter plant are set as

$$I_x = (1+\Delta_x)I_x^N, \quad I_y = (1+\Delta_y)I_y^N, \quad I_z = (1+\Delta_z)I_z^N,$$

where $\Delta_x = 0.1$, $\Delta_y = -0.1$, and $\Delta_z = 0.1$, corresponding to perturbations of $+10\%$, -10%, and $+10\%$ in the three inertia components, respectively. Therefore, the controller still uses the nominal values listed in Table 1, whereas the helicopter plant is simulated only with the perturbed inertia parameters.

The initial states of the helicopter are set as

$$\phi(0) = 0^\circ,\ \theta(0) = 0^\circ,\ \psi(0) = 0^\circ,\ p(0) = 0^\circ,\ q(0) = 0^\circ,\ r(0) = 0^\circ.$$

The commands of the attitude angles are set as

$$\phi_r = \begin{cases} 15^\circ & 0s \leqslant t \leqslant 10s; \\ 0^\circ & 10s < t \leqslant 20s; \end{cases} \quad \theta_r = \begin{cases} 0^\circ & 0s \leqslant t \leqslant 10s; \\ 15^\circ & 10s < t \leqslant 20s; \end{cases} \quad \psi_r = 10^\circ.$$

The constraints of the angular rates are set as

$$m_{\phi 1} = -45^\circ/s,\ m_{\phi 2} = 45^\circ/s;\ m_{\theta 1} = -45^\circ/s,\ m_{\theta 2} = 45^\circ/s;$$
$$m_{\psi 1} = -20^\circ/s,\ m_{\psi 2} = 20^\circ/s.$$

The environmental disturbances are set as

$$D_p = 1 - 1\sin(0.5\pi t)\ \ (N/m),\ D_q = -1 + 1\sin(0.5\pi t)\ \ (N/m),$$
$$D_r = 0.5 + 0.2\sin(0.25\pi t)\ \ (N/m).$$

The proposed composite dynamic gain controller (CDGC) is designed according to Eqs. (23), (10)–(12), and (27). The controller parameters and observer gains are designed as follows.

(1) Attitude control loop

$$k_{\phi 1} = 16,\ k_{\phi 2} = 64,\ l_\phi = 3,\ k_{\theta 1} = 16,\ k_{\theta 2} = 64,\ l_\theta = 3,$$
$$k_{\psi 1} = 16,\ k_{\psi 2} = 64,\ l_\psi = 2, l_{Ao1} = 5,\ l_{Ao2} = 5,\ l_{Ao3} = 2.$$

(2) Torque control loop

$$k_L = 8,\ k_M = 8.$$

Considering the parameters of the helicopter in Table 1, the specific form of the torque filter is as follows:

$$\hat{L}(s) = \frac{-708.02s - 2039.8}{De}p(s) + \frac{-55.86s - 2292.01}{De}q(s) + \frac{s + 10.01}{De}u_1 + \frac{5.02}{De}u_2,$$

$$\hat{M}(s) = \frac{11.45s - 650.39}{De}p(s) + \frac{-345.19s - 3505.33}{De}q(s) + \frac{1.08}{De}u_1 + \frac{s + 0.98}{De}u_2,$$

The denominator De of the torque filter is

$$s^2 + 20s + 94.5,$$

and the poles of denominator have negative real parts, and hence the torque filter is stable.

To validate the advantages of the proposed method, the following three methods were also carried out in the simulations, and they are designed as follows.

(1) Dynamic gain control (DGC)

$$\begin{cases} \tau_1 = -f_1 - k_{\phi 1}e_\phi - [k_{\phi 2} + \dfrac{l_\phi}{(m_{\phi 2} - \dot{e}_\phi)(\dot{e}_\phi - m_{\phi 1})}]\dot{e}_\phi,\ k_{\phi 1} = 16,\ k_{\phi 2} = 64, \\ \tau_2 = -f_2 - k_{\theta 1}e_\theta - [k_{\theta 2} + \dfrac{l_\theta}{(m_{\theta 2} - \dot{e}_\theta)(\dot{e}_\theta - m_{\theta 1})}]\dot{e}_\theta,\ k_{\theta 1} = 16,\ k_{\theta 2} = 64, \\ \tau_3 = -f_3 - k_{\psi 1}e_\psi - [k_{\psi 2} + \dfrac{l_\psi}{(m_{\psi 2} - \dot{e}_\psi)(\dot{e}_\psi - m_{\psi 1})}]\dot{e}_\psi,\ k_{\psi 1} = 16,\ k_{\psi 2} = 64. \end{cases}$$

(2) Composite nonlinear dynamic inverse control (CNDIC) based on the disturbance observer

$$\begin{cases} \tau_1 = -f_1 - \hat{D}_\phi - k_{\phi 1}e_\phi - k_{\phi 2}\dot{e}_\phi,\ k_{\phi 1} = 16,\ k_{\phi 2} = 64, \\ \tau_2 = -f_2 - \hat{D}_\theta - k_{\theta 1}e_\theta - k_{\theta 2}\dot{e}_\theta,\ k_{\theta 1} = 16,\ k_{\theta 2} = 64, \\ \tau_3 = -f_3 - \hat{D}_\psi - k_{\psi 1}e_\psi - k_{\psi 2}\dot{e}_\psi,\ k_{\psi 1} = 16,\ k_{\psi 2} = 64. \end{cases}$$

(3) Nonlinear dynamic inverse control (NDIC)

$$\begin{cases} \tau_1 = -f_1 - k_{\phi 1}e_\phi - k_{\phi 2}\dot{e}_\phi,\ k_{\phi 1} = 16,\ k_{\phi 2} = 64, \\ \tau_2 = -f_2 - k_{\theta 1}e_\theta - k_{\theta 2}\dot{e}_\theta,\ k_{\theta 1} = 16,\ k_{\theta 2} = 64, \\ \tau_3 = -f_3 - k_{\psi 1}e_\psi - k_{\psi 2}\dot{e}_\psi,\ k_{\psi 1} = 16,\ k_{\psi 2} = 64. \end{cases}$$

It is noteworthy that for a fair comparison, all four control methods (CDGC, DGC, CNDIC, and NDIC) share the same design of composite torque loop controller, and the comparative simulations are carried out under same conditions, including the UH's system parameters, initial states, environmental disturbances, and commands of attitude angles. In addition, the common controller gains are set to the same values across all compared methods, and the disturbance observer gains in CNDIC are kept identical to those in the proposed CDGC method.

Simulation results

Figure 3 shows the attitude angle tracking error responses under the proposed CDGC method and other three comparative methods (i.e., DGC, CNDIC, and NDIC). As shown in Fig. 3, both the proposed CDGC method and the conventional DGC method exhibit minimal initial fluctuations in attitude tracking error, with smooth response curves and no overshoot. Following a sudden change in the attitude angle command at 10 s, the proposed method and the CNDIC method achieve the fastest convergence of the tracking error; moreover, the proposed method shows the smallest fluctuation during the convergence. Figure 3 also indicates that the proposed CDGC method and the CNDIC method achieve the best steady-state tracking accuracy.

To quantitatively evaluate the tracking performance under continuous stochastic disturbances, the root mean square (RMS) of tracking error over the full simulation horizon is adopted as the performance metric. Compared with a fixed-threshold-based index, the RMS error provides a more consistent measure of the overall tracking accuracy because it accounts for both transient deviations and steady-state fluctuations. As shown in Table 2, CDGC achieves the lowest RMS errors across all three attitude channels (0.4939, 0.8199, and 0.2661 degrees for roll, pitch, and yaw, respectively), confirming the improved tracking accuracy of the proposed framework.

Table 1. Parameters of the Raptor-90 helicopter.

Parameter	m	I_x^N	I_y^N	I_z^N	Z_{col}	Z_w	L_a	L_b	M_a	M_b	A_{lon}	A_{lat}
Value	9.5	0.3	0.68	0.78	−9.60	−0.2	55.86	708.02	345.19	−11.45	−14.68	−5.57
Units	kg	$kg\cdot m^2$	$kg\cdot m^2$	$kg\cdot m^2$	–	–	–	–	–	–	–	–

m is the mass; I_x^N, I_y^N, I_z^N are the nominal value of the roll moment, pitch moment, and yaw moment; Z_{col}, Z_w, L_a, L_b, M_a, M_b, A_{lon}, A_{lat} are constant aerodynamic coefficients.

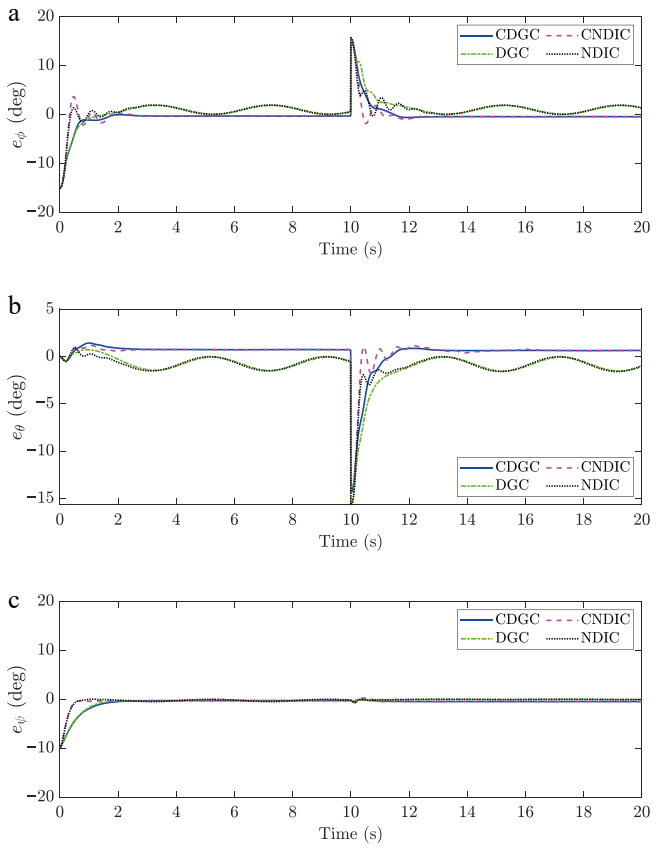

Fig. 3 Response of attitude angle tracking errors: (a) roll; (b) pitch; (c) yaw.

Table 2. RMS tracking error.

Method	e_ϕ	e_θ	e_ψ
CDGC	0.4939	0.8199	0.2661
DGC	1.2803	0.9508	0.2854
CNDIC	0.5307	0.8218	0.2743
NDIC	1.2732	0.9636	0.2979

CDGC denote the proposed composite dynamic gain controller; DGC denote dynamic gain controller; CNDIC denote composite nonlinear dynamic inverse controller; NDIC denote nonlinear dynamic inverse controller.

Figure 4 presents the attitude angular rate responses of the UH under the four control methods. It is observed that both the proposed CDGC method and the DGC method maintain the three-channel angular rates consistently within the prescribed constraint range, i.e., $\dot{\phi} \in [-45^\circ/s\ \ 45^\circ/s]$, $\dot{\theta} \in [-45^\circ/s\ \ 45^\circ/s]$, and $\dot{\psi} \in [-20^\circ/s\ \ 20^\circ/s]$. In contrast, the CNDIC and NDIC methods result in angular rate violations in all three channels, which verifies the superiority of the proposed approach in constraint handling.

As shown in Table 3, CDGC yields the smallest peak angular rates in all three axes, indicating that the proposed barrier-function-based dynamic gain effectively suppresses excessive angular rate excursions. In contrast, DGC, CNDIC, and NDIC produce larger peak rates, which implies that disturbance compensation alone or dynamic gain feedback alone cannot achieve the same level of transient rate moderation as the proposed composite design. In particular, CNDIC exhibits a higher peak roll rate because its disturbance-compensated inverse response is not equipped with the additional state-dependent damping effect introduced by the barrier gain.

Figures 5 and 6 illustrate the estimation performance of the torque loop filter and the attitude loop FTDOs, respectively. The

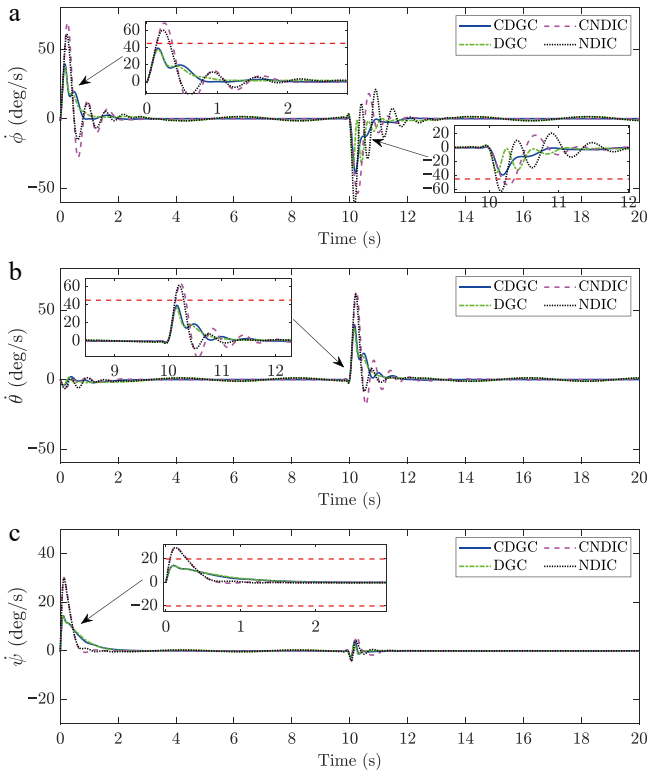

Fig. 4 Responses of attitude angular rates: (a) roll; (b) pitch; (c) yaw.

Table 3. Peak angular rate.

Method	$\dot{\phi}_{\max}$	$\dot{\theta}_{\max}$	$\dot{\psi}_{\max}$
CDGC	2.2035	1.0426	0.3246
DGC	2.9018	1.3920	0.5721
CNDIC	3.8262	1.3035	0.6007
NDIC	2.9753	1.3527	0.6076

CDGC denote the proposed composite dynamic gain controller; DGC denote dynamic gain controller; CNDIC denote composite nonlinear dynamic inverse controller; NDIC denote nonlinear dynamic inverse controller.

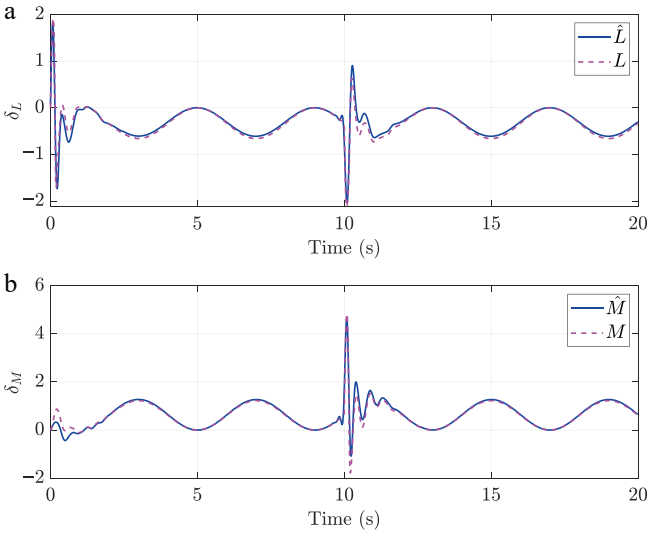

Fig. 5 Estimation of torques: (a) roll torque; (b) pitch torque.

results show that the FTDOs provide high-precision estimation of the lumped disturbances in the three channels of the attitude loop.

https://doi.org/10.48130/mav-0026-0022

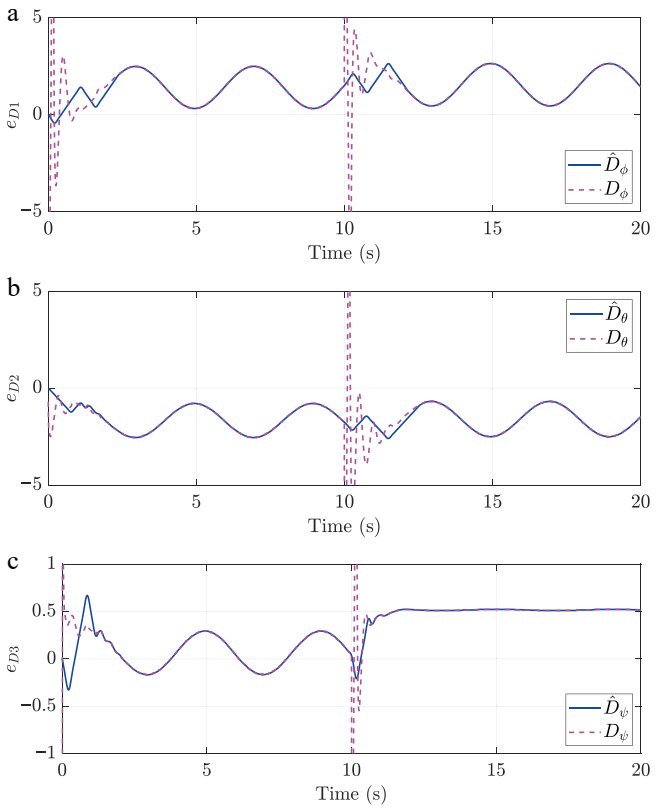

Fig. 6 Estimation of lumped disturbances: (a) roll; (b) pitch; (c) yaw.

Meanwhile, the torque loop filter achieves an accurate estimation of the roll and pitch moments while maintaining smooth estimation signals, which facilitates their direct integration into the controller.

Figure 7 illustrates the actual control inputs of the UH under the four control methods. It can be observed that during attitude command changes, the two composite methods (CDGC and CNDIC) achieve rapid dynamic adjustment and fast settling, ensuring high-precision tracking. Moreover, the two dynamic gain methods (CDGC and DGC) show significantly lower control amplitudes and smoother signals throughout the response compared with the other methods. In summary, the proposed CDGC method not only provides fast and accurate command tracking but also maintains smooth control actuation.

The control energy is evaluated as $E_i = \int_0^T \delta_i^2(t), \mathrm{d}t$, where δ_i denotes each control channel, $i \in \mathrm{lon}, \mathrm{lat}, \mathrm{ped}, \mathrm{col}$, and T is the total simulation duration. As shown in Table 4, CDGC has almost the same pedal and collective energy consumption as CNDIC, and both methods require substantially less energy in these two dominant channels than DGC and NDIC. The longitudinal and lateral cyclic energies are on the order of 10^{-7} for all methods and are negligible compared with the pedal and collective channels. Therefore, CDGC improves tracking accuracy and angular rate moderation without increasing the dominant control energy consumption.

Conclusions

This paper addresses the attitude tracking problem for small-scale UHs subject to multisource disturbances. A composite dynamic gain control scheme is developed, based on the fully actuated system theory. Compared with existing studies, this paper considers both angular rate constraints and the main rotor's flapping dynamics. The proposed method achieves -precision attitude tracking without violating the angular rate constraints. Simulation results based on a practical UH model further validate the effectiveness of the proposed method.

It should be noted that although the proposed controller explicitly constrains the angular rates, actuator saturation has not yet been incorporated into the theoretical control design. In addition, although measurement noise has been considered in the added robustness simulations, active noise suppression filtering has not

Table 4. Control energy consumption.

Method	δ_{lon}	δ_{lat}	δ_{ped}	δ_{col}
CDGC	3.0×10^{-7}	1.0×10^{-7}	0.0313	2.0898
DGC	2.4×10^{-7}	1.1×10^{-7}	0.0463	3.0956
CNDIC	3.2×10^{-7}	1.5×10^{-7}	0.0312	2.0896
NDIC	2.7×10^{-7}	1.4×10^{-7}	0.0460	3.0714

CDGC denote the proposed composite dynamic gain controller; DGC denote dynamic gain controller; CNDIC denote composite nonlinear dynamic inverse controller; NDIC denote nonlinear dynamic inverse controller.

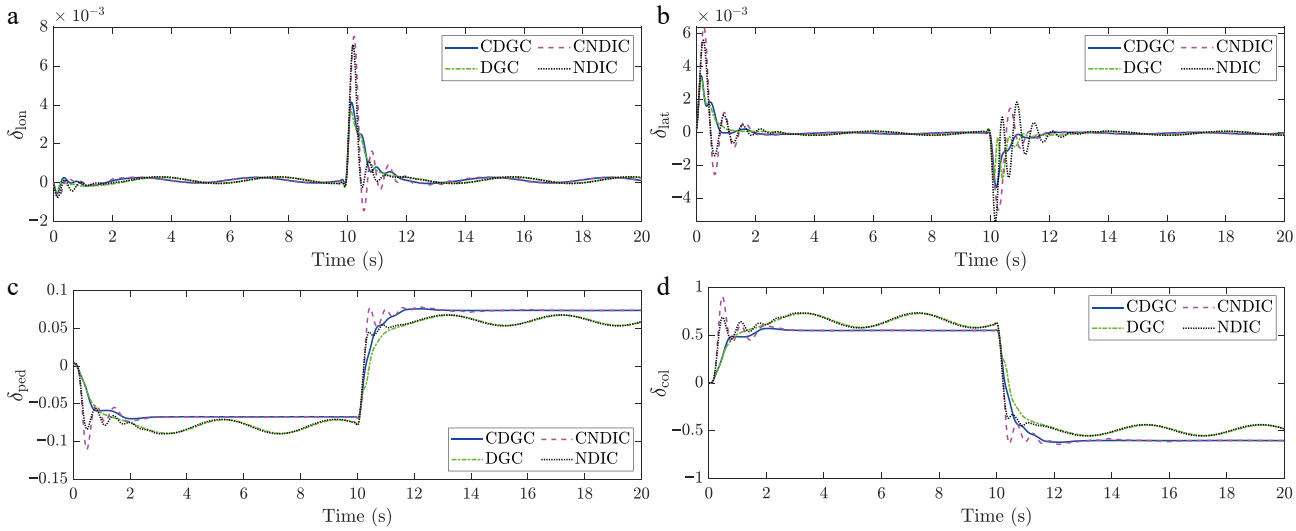

Fig. 7 Responses of actual control inputs: (a) longitudinal cyclic; (b) lateral cyclic; (c) tail rotor control; (d) collective.

been integrated into the present observer–controller framework. Future work will therefore focus on extending the proposed method to saturation-aware attitude control and on embedding dedicated noise attenuation mechanisms into the observer-based design, so as to further enhance its practical applicability and robustness in realistic flight environments.

Author contributions

The authors confirm contribution to the paper as follows: study conception and design: Kong Z, Zhao Z; data collection: Li P, Li F; analysis and interpretation of the results: Kong Z, Zhao Z; draft manuscript preparation: Kong Z, Li P. All authors reviewed the results and approved the final version of the manuscript.

Data availability

Data sharing is not applicable to this article, as no datasets were generated or analyzed during the current study.

Acknowledgments

This work is supported in part by the Science Center Program of the National Natural Science Foundation of China under Grant No. 62188101, the Natural Science Foundation of Jiangsu Province (No. BK20230091), and the National Natural Science Foundation of China (No. 62573230).

Conflict of interest

The authors declare that they have no conflict of interest.

Dates

Received 16 April 2026; Revised 18 June 2026; Accepted 7 September 2026; Published online 12 October 2026

References

[1] Ma A, Xian B, Liu M, Yuan B, Jin X. 2025. Adaptive robust fault-tolerant control for a small size unmanned helicopter: theory and experimental implementation. *Aerospace Science and Technology* 160:110059

[2] Wang H, Shi S, Zhen Z. 2025. Flexible performance-based predefined-time tracking control for unmanned helicopter with irregular constraints. *Aerospace Science and Technology* 164:110445

[3] Wang H, Shi S, Zhen Z. 2024. Disturbance observer based fixed-time tracking control for unmanned aerial helicopters. *Journal of the Franklin Institute* 361(16):107184

[4] Wan M, Yong K. 2025. Manoeuvrability limitation-based flight control for unmanned autonomous helicopter with state constraints and input saturation. *IET Control Theory & Applications* 19(1):e70094

[5] Li S, Yang J, Chen W, Chen X. 2014. *Disturbance Observer-Based Control: Methods and Applications*. Boca Raton: CRC Press. pp. 1–340 doi: 10.1201/b16570

[6] Ma H, Chen M, Yang H, Wu Q, Chadli M. 2021. Switched safe tracking control design for unmanned autonomous helicopter with disturbances. *Nonlinear Analysis: Hybrid Systems* 39:100979

[7] Wang X, Li Z, Yu X, He Z. 2022. Adaptive smooth disturbance observer-based fast finite-time attitude tracking control of a small unmanned helicopter. *Journal of the Franklin Institute* 359(11):5322–5340

[8] Lai Y, Le T. 2021. Adaptive learning-based observer with dynamic inversion for the autonomous flight of an unmanned helicopter. *IEEE Transactions on Aerospace and Electronic Systems* 57(3):1803–1814

[9] Li T, Zhao Z, Ding S, Su J. 2024. Composite controller design for quadrotor UAVs with uncertainties and noises based on combined Kalman filter and GPIO. *IEEE Transactions on Aerospace and Electronic Systems* 60(1):882–892

[10] Li Y, Huang Y, Li D, Sun Y, Liu H, et al. 2023. Flight tracking control for helicopter attitude and altitude systems using output feedback method under full state constraints. *Aerospace* 10(8):696

[11] Hua C, Chen J, Guan X. 2019. Dynamic surface based tracking control of uncertain quadrotor unmanned aerial vehicles with multiple state variable constraints. *IET Control Theory & Applications* 13(4):526–533

[12] Li R, Chen M, Wu Q. 2018. Robust control for an unmanned helicopter with constrained flapping dynamics. *Chinese Journal of Aeronautics* 31(11):2136–2148

[13] Feng Y, Zhou Y, Ho HW. 2024. Reinforcement learning based robust tracking control for unmanned helicopter with state constraints and input saturation. *Aerospace Science and Technology* 155:109549

[14] Ma H, Chen M, Wu Q. 2023. Disturbance observer-based safe tracking control for unmanned helicopters with partial state constraints and disturbances. *IEEE/CAA Journal of Automatica Sinica* 10(11):2056–2069

[15] Duan G R. 2021. High-order fully actuated system approaches: Part I. *Models and basic procedure. International Journal of Systems Science* 52(2):422–435

[16] Hachem M, Miquel T, Bronz M, Roos C. 2025. Trajectory optimization for fully actuated hexacopters: enhancing maneuverability and applications. *International Journal of Micro Air Vehicles* 17:1–8

[17] Cui K, Duan G, Hou M. 2024. Discrete-time model reference tracking control for a class of combined spacecraft: a high-order fully actuated system approach. *IEEE Transactions on Automation Science and Engineering* 21(4):6966–6977

[18] Tang S, Zheng Z, Qian S, Zhao X. 2014. Nonlinear system identification of a small-scale unmanned helicopter. *Control Engineering Practice* 25:1–15

[19] Cai G, Chen B, Lee TH, Lum KY. 2012. Comprehensive nonlinear modeling of a miniature unmanned helicopter. *Journal of the American Helicopter Society* 57(1):1–13

[20] Levant A. 2003. Higher-order sliding modes, differentiation and output-feedback control. *International Journal of Control* 76(9–10):924–941

[21] Huang Y, Zhang W. 2002. Development of active disturbance rejection controller. *Control Theory and Applications* 19(4):485–492

[22] Khalil HK. 1996. *Nonlinear Systems*. 2nd. edition. Upper Saddle River, NJ: Prentice Hall. https://search.worldcat.org/title/33358773

Copyright: © 2026 by the author(s). Published by Maximum Academic Press, Fayetteville, GA. This article is an open access article distributed under Creative Commons Attribution License (CC BY 4.0), visit https://creativecommons.org/licenses/by/4.0/.